



Simplify your imaging workflows

**Make research imaging workflows accessible, traceable,
and secure with Athena Software for Core Imaging Facilities.**

Thermo Scientific™ Athena Software is a premium imaging data management platform designed for core imaging facilities that support materials science research.

Athena Software ensures traceability of images, metadata, and experimental workflows through an intuitive and collaborative web interface.

Find out more at thermofisher.com/athena

ThermoFisher
SCIENTIFIC

Efficient Luminescent Solar Concentrators Based on Environmentally Friendly Cd-Free Ternary AIS/ZnS Quantum Dots

Lorena Dharmo, Francesco Carulli, Philip Nickl, Karl David Wegner, Vasile-Dan Hodoroaba, Christian Würth, Sergio Brovelli, and Ute Resch-Genger*

Luminescent solar concentrators (LSC) allow to obtain renewable energy from building integrated photovoltaic systems. As promising efficient and long-term stable LSC fluorophores semiconductor nanocrystals like quantum dots (QDs) with size and composition tunable optoelectronic properties have recently emerged. The most popular II/VI or IV/VI semiconductor QDs contain, however, potentially hazardous cadmium or lead ions, which is a bottleneck for commercial applications. A simple aqueous based, microwave-assisted synthesis for environmentally friendly and highly emissive AgInS₂/ZnS QDs is developed using 3-mercaptopropionic acid (MPA) and glutathione (GSH) and their incorporation into poly(laurylmethacrylate) (PLMA) polymer slabs integrable in LSC devices (10.4 × 10.4 × 0.2 cm³, G = 12.98). With this simple approach, optical power efficiencies (OPE) of 3.8% and 3.6% and optical quantum efficiencies (OQE) of 24.1% and 27.4% are obtained, which are among the highest values yet reported.

technologies like photovoltaic (PV) devices can be used in densely populated urban areas.^[1] The energy efficiency and energy production costs of meanwhile affordable silicon-based PV cells can be improved by the luminescent solar concentrator (LSC) technology,^[2] providing transparent or semi-transparent building integrated photovoltaic materials (BIPV)^[3] for windows,^[4,5] buildings,^[6] facades, and roof tops.^[7]

A typical LSC consists of fluorophores embedded in a transparent optical waveguide that absorb direct and diffuse sunlight and emit photons at longer wavelengths.^[1b,3] The re-emitted light is guided by total internal reflection (TIR) to the waveguide edges where it is converted into electrical power by small PV

cells installed along the LSC slab perimeter.^[4] Other advantages of LSCs include a reduced total amount of PV material, lower production costs, and an enhanced efficiency due to a larger active area of the solar cells. First, organic dyes like rhodamines, coumarins, and perylenes with high photoluminescence (PL) quantum yields (QYs) were used in LSCs.^[1b] These dyes suffer from a considerable spectral overlap between their absorption and emission bands,^[8] harvest light only from a relatively small fraction of the solar spectrum, have a poor photostability, and show a poor spectral match between their emission and the spectral response of Si-based PV solar cells, limiting LSC efficiency. Principally interesting alternatives are perovskites^[9] and Cd- and Pb-based semiconductor quantum dots (QDs),^[10,4,11,12] which outperform organic dyes due to their broad absorption bands, high molar extinction coefficients, high PL QY, emission in a spectral window where PV cells have an optimum energy conversion efficiency, and excellent photochemical stability. However, recent restrictions by the European Union (Restriction of Hazardous Substances directive; Directive 2011/65/EU) of utilizing potentially toxic cadmium and lead^[13] in commercial applications triggered the search for eco-friendly alternative nanomaterials like carbon dots,^[9c,14] gold nanoclusters, InP QDs,^[15] silicon QDs,^[16] and heavy-metal free QDs such as CuInS₂ (CIS) or AgInS₂ (AIS) QDs. Particularly interesting are Cu-based and AIS QDs with their broad absorption spectra, Stokes-shifted broad PL spectra in the visible and near-infrared (NIR) region, and high PL QY,^[17] that are accessible in high quality by aqueous syntheses.^[18] For example, a

1. Introduction


With increasing concerns about global warming and environmental sustainability using traditional energy production approaches, advanced eco-friendly and efficient power

L. Dharmo, P. Nickl, Dr. K. D. Wegner, Dr. C. Würth, Dr. U. Resch-Genger
Division Biophotonics
Federal Institute for Materials Research and Testing (BAM)
Richard Willstätter Straße 11, 12489 Berlin, Germany
E-mail: Ute.Resch@bam.de

L. Dharmo
Department of Physics
Humboldt Universität zu Berlin
Newtonstraße 15, 12489 Berlin, Germany

Dr. F. Carulli, Prof. S. Brovelli
Department of Materials Science
University of Milano–Bicocca
Via Roberto Cozzi 55, Milan 20125, Italy

Dr. V.-D. Hodoroaba
Department of Materials Chemistry
Federal Institute for Materials Research and Testing (BAM)
Unter den Eichen 87, 12203 Berlin, Germany

 The ORCID identification number(s) for the author(s) of this article can be found under <https://doi.org/10.1002/adom.202100587>.

© 2021 The Authors. Advanced Optical Materials published by Wiley-VCH GmbH. This is an open access article under the terms of the Creative Commons Attribution License, which permits use, distribution and reproduction in any medium, provided the original work is properly cited.

DOI: 10.1002/adom.202100587

power conversion efficiency (PCE) of 8.71% was obtained with CIS QDs in polymethylmethacrylate (PMMA),^[19,20] and optical efficiencies (η) of 3.27% and 6.97% with poly(2-vinylpyridine) (PVP)-CuInSeS QD LSCs^[21] and CIS QDs doped with Zn and Al, respectively.^[22] Ag-based ternary QDs like AIS have been barely assessed as LSC chromophores except for a single device utilizing AIS QDs prepared in organic solvents with hazardous chemicals.^[17a]

Here, we present a simple, environmentally friendly approach to AIS-based LSCs using AIS/ZnS QDs prepared in water with glutathione (GSH) or 3-mercaptopropionic acid (MPA) as surface ligands, followed by ligand exchange for hydrophobic oleylamine (OLA) and oleic acid (OA). Photopolymerization of lauryl methacrylate (LMA) and ethylene glycol dimethacrylate (EGDM) in the presence of these hydrophobic AIS/ZnS QDs yielded highly fluorescent AIS/ZnS-PLMA-LSCs with optical power efficiencies (OPE) of 3.8% and 3.6% ($10.4 \times 10.4 \times 0.2 \text{ cm}^3$, geometry factor $G = 12.98$)

2. Experimental Section

2.1. Materials

Silver nitrate (Honeywell, 99.8%), indium(III) chloride (Sigma–Aldrich, 98%), reduced L-glutathione (Sigma–Aldrich), 3-mercaptopropionic acid (AppliChem), sodium sulphide (Abcr, 98% Na₂Sx9H₂O), ammonia 5.0 M (Sigma–Aldrich), citric acid (Roth, 99.5%), zinc acetate (Chemsolute, 99.5% Zn(CH₃COO)₂ × 2H₂O), ethanol (absolute, Merck), toluene (spectroscopic grade, Merck), oleylamine (AppliChem, 70–80%), oleic acid (Sigma–Aldrich, 90% technical grade), lauryl methacrylate (Sigma–Aldrich, 96%), 2,2-dimethoxy 2-phenyl acetophenone (Sigma–Aldrich), and ethylene glycol dimethacrylate (Sigma–Aldrich, 98%). All chemicals and solvents were used as received.

2.2. Synthesis

2.2.1. Core GSH-Capped AIS QDs

The synthesis of ternary GSH-capped AIS core QDs was performed according to a procedure from Stroyuk et al.^[23] To a solution containing 13 mL deionized water, 4 mL of indium(III) chloride (1.0 M) solution (containing 0.25 M nitric acid to avoid In³⁺ hydrolysis) and 12 mL of glutathione (GSH) solution (0.5 M) were added. Subsequently, 0.5 mL ammonia solution (5.0 M) was added under vigorous stirring followed by the addition of 10 mL of silver nitrate (0.1 M), 5 mL of sodium sulphide (1.0 M), and 1 mL of citric acid (2.0 M). The reaction mixture was then heated to 100 °C for 45 minutes using a heating mantel.

2.2.2. ZnS Shelling of GSH-Capped AIS/ZnS QDs

To grow a ZnS shell, the as-prepared AIS core QDs were added to a mixture consisting of 15 mL of GSH (0.5 M), 2 mL

of ammonia solution (5.0 M), and 8 mL of zinc acetate (1.0 M) (containing 0.01 M nitric acid). The shell growth was initiated by heating the reaction mixture to 100 °C for 20 min using a heating mantel.

The core/shell AIS/ZnS QDs were purified by addition of 75 mL of ethanol and centrifugation at 10 000 rpm for 5 min to precipitate the QDs. The precipitated QDs were then redispersed in 10 mL deionized water to obtain a colloidal stable dispersion of GSH-capped AIS/ZnS QDs.

2.2.3. Core MPA-Capped AIS QDs

MPA-capped AIS/ZnS QDs were synthesised by transferring the synthesis of GSH capped AIS/ZnS to a microwave (MW) assisted procedure and substituting GSH by MPA. To a MW vessel containing 4.33 mL deionized water, 3.33 mL of silver nitrate (0.1 M), 4 mL MPA (0.5 M), 3.5 mL ammonia solution (6.7 M), 0.33 mL of citric acid (2.0 M), and 1.33 mL indium(III) chloride (1.0 M) (containing 0.1 M nitric acid) (redispersed by addition of an ammonia solution) were added under stirring. The pH of the reaction mixture was controlled to be between 8 and 9, and finally 1.67 mL of sodium sulphide (1.0 M) was quickly added under vigorous stirring. The reaction vessel was then heated to 100 °C in the microwave and kept at this temperature for 50 min.

2.2.4. ZnS Shelling of MPA-Capped AIS/ZnS QDs

For the ZnS shelling procedure, 5 mL MPA (0.5 M), 3 mL ammonia solution (0.5 M), and 2.67 mL containing 0.01 M nitric acid zinc acetate (1.0 M) (redispersed by addition of ammonia solution) were added to the dispersion containing AIS QDs under vigorous stirring. The mixture was then heated to 100 °C for 30 min.

Finally, the QD dispersion was concentrated to 10 mL by evaporation of the solvent using a rotary evaporator and redispersing the QDs in 10 mL deionized water.

2.2.5. Phase Transfer

Ligand exchange of the hydrophilic surface ligands MPA and GSH, required to enable the dispersibility of the initially prepared hydrophilic AIS/ZnS QDs in apolar organic solvents like toluene and the monomers LMA and EGDM, was performed according to a procedure from Stroyuk et al.^[24] For this purpose, 10 mL of an aqueous dispersion of thiol-capped AIS/ZnS QDs was mixed with 10 mL toluene, 10 mL oleylamine (OLA), 2.5 mL oleic acid (OA), and 2.5 mL ethanol. The mixture was shaken for 2 min. and subsequently centrifuged at 10 000 rpm for 5 min. The toluene fraction obtained by separation of the two liquid phases was decanted and 40 mL ethanol was added to precipitate the QDs from the organic phase. A final centrifugation step was performed (10 000 rpm for 2 min) to yield a pellet of OLA/OA-capped QDs, which was then suspended in 10 mL of toluene to obtain a colloidal stable suspension of OLA/OA-capped QDs.

2.2.6. Fabrication of QD-PLMA LSC

For the fabrication of the LSC, a mixture of 0.06% (w/w) dried OLA/OA-capped AIS/ZnS QDs (with 20 μL of OA), 80% LMA (w/w) and 20% EGDM (w/w)^[16] was prepared. This mixture was sonicated and stirred until the QDs were homogeneously dispersed. Then, 250 ppm of the polymerization initiator 2,2-dimethoxy-2-phenyl acetophenone (Irgacure 651) was added and the mixture was stirred for 30 min. The solution was then poured into a mold made by two glass sheets separated by a polymeric spacer. The polymerization was initiated by illumination with UV light (365 nm, 20 W) for 40 min at room temperature. After being kept in the dark for further 30 min, the QD-containing polymer slab was removed from the mold and polished.

2.3. Methods

2.3.1. Structural Characterization

TEM Measurements: TEM measurements were performed with a scanning transmission electron microscope Fei Titan 80–300 (FEI, Hillsboro, OR, USA) at 300 kV.

XRD Measurements: X-ray diffraction (XRD) measurements were done with a Rigaku Ultima IV diffractometer (Rigaku, Tokyo, Japan) with Cu $K\alpha$ radiation ($\lambda = 0.15406$ nm).

EDX Measurements: Energy-Dispersive X-ray spectroscopy (EDX) measurements were performed with a Thermo Fisher Scientific system (Waltham, MA, USA) of type silicon-drift detector (SDD) UltraDry with a nominal detector area of 100 mm². The measurement software was Pathfinder 1.3. The EDS system was attached to a Zeiss Supra 40 SEM (Zeiss, Oberkochen, Germany) with a Schottky-field emitter. Each sample was analyzed on three different areas of about 100 \times 100 μm^2 at an excitation energy of 10 keV and a mean value for the elemental composition had been calculated for each sample. S $K\alpha$ (2.31 keV), Zn $L\alpha$ (1.01 keV), Ag $L\alpha$ (2.98 keV), and In $L\alpha$ (3.29 keV) X-ray lines had been quantified.

2.3.2. Optical-Spectroscopic Characterization

Absorption Spectra: The absorption spectra were measured with a calibrated double beam spectrometer Specord 210plus (Analytik Jena) in a wavelength range of 200–800 nm using an integration time of 0.5 s nm⁻¹.

PL Spectra: Steady-state fluorescence emission spectra were recorded with a calibrated fluorometer FLS 920 (Edinburgh Instruments) equipped with a Xenon lamp, using excitation wavelengths of 400, 450, and 500 nm, respectively. The integration time was set to 0.5 s and three scans were done per measurements.

PL Decay Kinetics: The PL decay kinetics of the QDs in dispersion and embedded in the polymer were measured at different excitation and emission wavelengths with the fluorometer FLS 920 (Edinburgh Instruments) equipped with a pulsed EPLED laser (wavelength of 375 \pm 5 nm; pulse duration of 60 ps, and pulse repetition rate of 100 kHz equalling one pulse every

10 μs) and detected with a multichannel plate (MCP) detector using time-correlated single-photon counting (TCSPC). The multiexponential decay curves were evaluated using the software FAST (Edinburgh Instrument) and could be fitted with a tri-exponential reconvolution fit, thereby considering the instrument response function (IRF) determined with a scatterer. Intensity-weighted and amplitude-weighted average lifetimes were calculated from the fitted multi-exponential decay curves as shown in Equation (S1), Supporting Information.

Photoluminescence Quantum Yields (PL QY): PL QY values were determined absolutely using the commercial calibrated integrating sphere setup Quantaury-QY C11347-11 (Hamamatsu) previously evaluated by the authors.^[25] PL QY measurements of dispersed QDs were performed at room temperature in 10 \times 10 mm long neck quartz cuvettes from Hamamatsu, while the QD-doped polymers were cut into pieces that fit into a round quartz cuvette with a diameter of 2 cm and a thickness of 5 mm from Hellma GmbH.

LSC Efficiency Measurements: The efficiency of the LSC devices was evaluated using a calibrated solar simulator with power density $P = 100$ mW cm⁻² (1.5 AM Global). The tested LSCs were coupled with a Si-solar cell. Initially PL emitted from the LSC edge was collected with a spectrometer to evaluate the real spectral photon distribution. Such profile was successively scaled for the efficiency of the calibrated photodiode to evaluate the real number of re-emitted photons reaching the LSC edges which enabled the authors to finally calculate the OPE and quantum optical efficiency (QOE). All experiments were carried out without the use of back reflector or back diffuser at the bottom of the waveguide. The scattering losses were determined by light propagation experiments, using a 405 nm laser as excitation light source for all device lengths and collecting the light at one of the edges.

2.4. Results and Discussion

2.4.1. Structural Analysis

The two types of ternary AIS/ZnS QDs, synthesized using either MPA or GSH as stabilizing ligands and a constant ratio of Ag : In : S : Zn : ligand, 0.25 : 1 : 1.25 : 2 : 6.77, were initially prepared in water following the procedures described in the experimental section. To incorporate AIS/ZnS QDs into a polymer matrix, the ligands of the prepared water-soluble AIS/ZnS QDs were replaced with long aliphatic chains (OLA and OA) to make the QDs dispersible in non-polar organic solvents. This involved a phase transfer of the AIS/ZnS QDs from water to toluene following an established protocol from Stroyuk et al.^[24] Whether this type of phase transfer led to a complete exchange of all surface ligands or to a mixture of different surface ligands was not further examined. In the following discussion, we refer to the QDs after ligand exchange to GSH-OLA/OA and MPA-OLA/OA QDs.

The size, composition, and crystal phase of the resulting OLA- and OA-capped AIS/ZnS QDs were characterized by X-ray diffraction (XRD), transmission electron microscopy (TEM), and energy-dispersive X-ray spectroscopic (EDX) measurements. The diffraction pattern of both QDs (in **Figure 1c**)

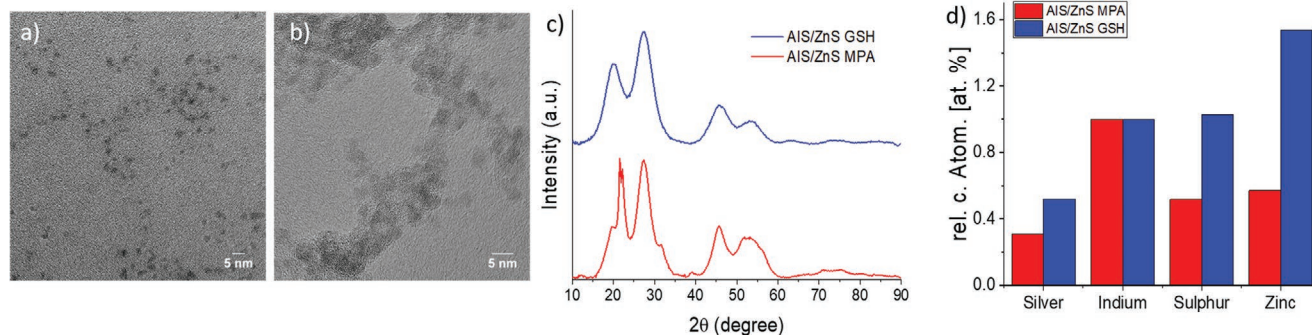


Figure 1. TEM measurements of a) AIS/ZnS QDs GSH-OLA/OA capped and b) MPA-OLA/OA capped; c) XRD measurements of AIS/ZnS QDs GSH-OLA/OA and MPA-OLA/OA capped; d) EDX atomic concentration normalized to the indium concentration of AIS/ZnS QDs, capped with GSH-OLA/OA and MPA-OLA/OA.

exhibit three broad peaks at matching positions compatible with the indices for the (112), (204), and (312) planes of tetragonal chalcopyrite AgInS_2 . As indicated by the broad diffraction peaks, the QDs are $\approx 2\text{--}4$ nm, which was confirmed by TEM measurements in Figure 1a,b; and Figure S1, Supporting Information. The EDX measurements (Figure 1d) reveal that the GSH-OLA/OA QDs contain a rather similar Ag:In:S:Zn ratio of 0.5:1.0:1.0:1.5 as initially used for the synthesis of the QDs. The element composition of the MPA-OLA/OA QDs is, however, deficient in S and Zn. This suggests slightly different surface chemistries of both types of AIS QDs and/or a different growth mechanism of the ZnS shell.

2.4.2. Optical Properties of AIS/ZnS QDs

The absorption spectra of the GSH-OLA/OA and MPA-OLA/OA QDs shown in Figure 2 are typical for ternary AIS/ZnS QDs, revealing a broad unstructured shape lacking the sharp excitonic feature observed for binary QD systems. The PL spectra are broad with a full width at half-maximum (FWHM) of ≈ 200 nm (520 meV), which considerably exceeds the FWHM values of the PL bands of binary II/VI or III/V QDs such as CdSe and InP QDs.^[26] The broad PL bands can be attributed to different PL mechanisms such as the radiative recombination of donor–acceptor pairs, the self-trapped exciton model, the recombination of a localized hole with a conduction band electron or a combination of these mechanisms, which is still debated.^[17b,23–24,27] The surface ligand used for QD synthesis seems to significantly influence the spectral position of the PL maximum as suggested by the redshift of the PL maximum from 590 to 700 nm observed for MPA in comparison to GSH. Similar results were obtained by Stroyuk et al.^[24] with TGA-stabilized AIS QD that exhibited also a bathochromically shifted PL compared to GSH-capped AIS QDs. The observed average PL dynamics are also affected by the surface ligand as revealed by the PL decay curves shown in Figure 2g with amplitude-weighted average lifetimes of 360 and 700 ns obtained for GSH-capped and MPA-capped AIS/ZnS QDs, respectively. The corresponding PL decay curves and resulting fits are shown in Figure 2g,h,i and the used equations and calculated lifetimes can be found in Table S1, Supporting Information. The observed differences in the photophysical properties can be

ascribed to the influence of the surface ligand, that is, MPA, or GSH, molecules on the core and core/shell QDs during their formation, leading to slightly different chemical compositions and slightly different surface chemistries as described in the previous section. Nevertheless, the PL QY of the GSH-capped QDs of 60% closely match the PL QY of the MPA-capped AIS/ZnS QDs of 64%. A more detailed investigation of the influence of the surface ligand on the optical properties of the QDs was beyond the scope of this study, focusing on AIS/ZnS-based LSCs.

The absorption spectra shown in Figure 2d,e closely match before and after phase transfer. The PL maxima are, however, red-shifted by 6 nm for GSH-OLA/OA and blue-shifted by 17 nm for MPA-OLA/OA upon phase transfer. For both QD types, ligand exchange and phase transfer lead to increased PL QY values of 70% and 74% of the subsequently formed GSH-OLA/OA- and MPA-OLA/OA-capped AIS/ZnS QDs. As the FWHM of the PL bands undergo only minor changes and the PL QY values are even increased, a degradation of the QDs during this procedure can be excluded. The observed moderate changes in the optical properties of the QDs are ascribed to the influence of the OLA and OA ligands that coordinate to the QD surface atoms with their amino or carboxylic groups whereas MPA and GSH interact with the QD surface ions via their thiol functionalities. This assumption is also supported by the decrease of the average PL lifetime of the MPA-OLA/OA QDs from initially 700 to 520 ns and from 360 to 270 ns for GSH-OLA/OA QDs. The PL decay kinetics of both AIS/ZnS QDs are shown in Figure 1h and the fit results are given in Table S2, Supporting Information. Both AIS/ZnS QDs are colloidal stable for at least 2 years after ligand and phase transfer preserving a constant PL QY of 70% (see Figure S2, Supporting Information).

Subsequently, the AIS/ZnS QDs were embedded in a PLMA matrix, which was chosen due to its high compatibility, excellent optical properties, and well reproducible photopolymerization. The photographs of the obtained LSC slabs presented in Figure 3a,b highlight the homogeneous dispersion of the QDs in the polymer matrix. The devices are transparent and slightly colored, with the total transmittance of both samples exceeding 85% (see Figure S3, Supporting Information). This underlines the good quality of the devices and their suitability for LSC technology.^[28] The absorption and emission spectra

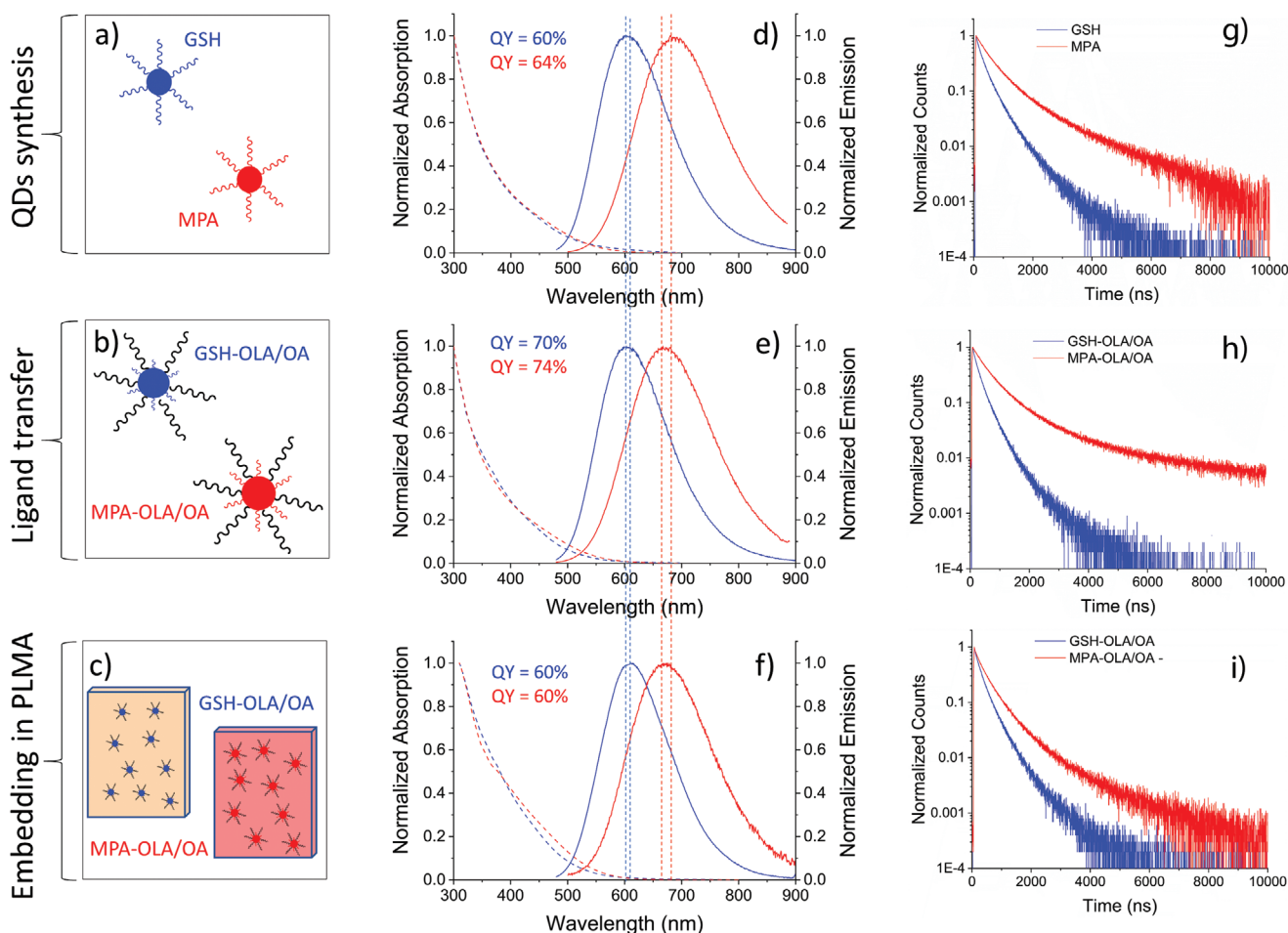


Figure 2. Schematic presentation of the a) hydrophilic AIS/ZnS QDs capped with MPA and GSH, b) after ligand exchange yield, the corresponding hydrophobic AIS/ZnS QDs capped with MPA-OLA/OA or GSH-OLA/OA, and c) hydrophobic AIS/ZnS QDs embedded in a polymer matrix. Normalized absorption and emission spectra and PL decay curves of the AIS/ZnS QDs prepared using MPA (red line) and GSH (blue line) after synthesis in water (d), (g); after ligand exchange with OLA/OA and phase transfer in toluene (e), (h); and in PLMA after the polymerization process (f), (i), respectively.

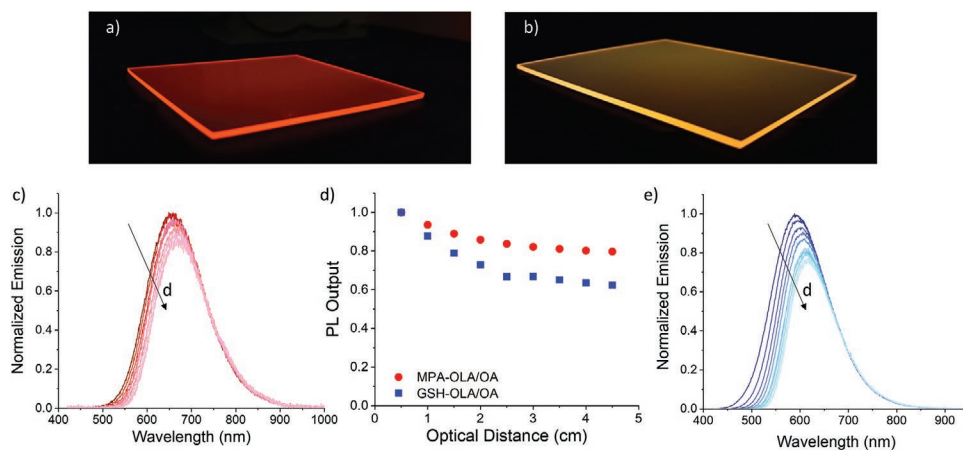


Figure 3. Photographs of the LSC waveguides (PLMA, wt. 0.06% QD concentration) prepared with a) MPA-OLA/OA-capped AIS/ZnS and b) GSH-OLA/OA-capped AIS/ZnS QDs. Normalized PL emission spectra of c) MPA-OLA/OA AIS/ZnS QDs and e) GSH-OLA/OA AIS/ZnS QDs in PLMA collected at the edge of the polymer slab with an excitation light source located at increasing distances ($d = 0.5$ cm) from the collector edge of the polymer slab; d) Overall reabsorption of the LSC samples.

shown in Figure 2e,f closely resemble the respective spectra of the QDs dispersed in toluene. The PL QY of the GSH-OLA/OA AIS/ZnS QDs only drops by 2% to 70%, whereas the PL QY of the MPA-OLA/OA QDs increases to 74%. These high PL QY values exceed the PL QY values reported by Chen et al. by a factor of 2.^[17a] Also, changes in the average PL lifetimes are observed, that is, a slight increase to 282 ns for the GSH-OLA/OA AIS/ZnS QDs and a drop to 330 ns for the MPA-OLA/OA QDs (see Figure 2i, see also Table S3, Supporting Information). Apparently, the optical properties of MPA-OLA/OA QDs are more strongly influenced by their environment and ligand shell. One possible explanation could be the different strength of the bonds between the QD surface atoms and the ligand molecules, as MPA bears only a single SH group and GSH a SH and a NH group that can coordinate to the QD surface. This could subsequently affect the ligand shell resulting after ligand exchange and phase transfer and hence, the QD surface.

To obtain a first insight into the stability of AIS/ZnS QDs in an organic solvent, we compared the optical properties of the freshly prepared and aged samples, that is, the corresponding toluene stock solutions stored at room temperature in the dark for two years (see Figures S2 and S4, and Table S4, Supporting Information). The samples show slightly modified emission spectra and a change in the calculated average amplitude-weighted PL decays (but the PL QY values remain constant). Fresh LSCs were prepared from the same AIS/ZnS QDs batch kept in aerated toluene dispersion in the dark at room temperature for one year and the performance of the resulting LSCs was compared. As shown in Figure S2, Supporting Information, the absorption and emission spectra obtained after embedding the freshly prepared and aged QDs in a PLMA matrix closely match. Also, for the LSC prepared from the aged AIS/ZnS QDs, we still observe a PL QY of 60% after incorporation into the polymer. Hence, the influence of the polymerization process on the PL QY of the QD-polymer composite material is negligible. Moreover, this match underlines the robustness of the QDs and the reproducibility of the polymerization procedure. This excellent long-term stability of the QD dispersions is very beneficial for the application of these materials and will be systematically assessed in the future under different application-relevant ambient storage conditions.

2.4.3. Efficiency and Loss Studies of AIS/ZnS Embedded LSCs

To evaluate the efficiency of the AIS/ZnS-based LSCs, we examined the optical losses due to reabsorption and matrix effects that can affect LSC performance, on the basis of the absorption and emission spectra of the AIS/ZnS QDs. Reabsorption losses are determined by the spectral overlap between absorption and emission bands that correlate with the size of the effective Stokes shift. A small Stokes shift can considerably hamper the overall performance of a LSC device by the reabsorption and randomization of the emitted photons, which are the main loss mechanisms in LSC. Reabsorption reduces the overall efficiency of a LSC device as the PL QY of the emitters are below unity, while photon randomization increases the probability of a photon to escape from the large area faces of the waveguide instead of being concentrated at the edges. To quantify reabsorption losses

and to confirm the uniformity of the optical properties of the QD-doped polymerization product, we studied the dependence of the PL spectra and the relative PL intensity on the distance travelled by light inside the LSCs. The PL spectra collected at the LSC edge for increasing distances from the incident excitation light spot (distance between the excitation light spot and the LSC edge being varied from 0 to 5 cm in steps of 5 mm) are shown in the Figure S5, Supporting Information. The observed drop of the overall PL intensity with distance is the result of the combined effects of increasing reabsorption and decreasing collection efficiency (see Figure S6, Supporting Information). To assess solely the contribution of the former effects, the PL spectra were normalized in the low energy region of the PL spectra, where the overlap between absorption and PL is negligible.^[25b] The resulting PL spectra and the PL intensities summarized in Figure 3 reveal only small changes in the PL spectral shape with increasing distance. This points to overall losses of up to 31% for GSH-OLA-OA capped QDs and 18% for MPA-OLA/OA capped QDs in the LSCs, respectively. This is ascribed to the redshift in PL obtained with the MPA ligands, that shifts the PL band further away from the onset of QD absorption.

As shown in Figure 3a,b, under UV illumination, the QD emission is efficiently guided to the edges of the LSC as required for the desired application. To quantify the efficiency of the LSCs based on GSH-OLA/OA and MPA-OLA/OA AIS/ZnS QDs, we determined the OPE,^[18,19] defined as the ratio of the optical power emitted at the LSC edges and the incident power, and the OQE, defined as the ratio of the number of photons emitted from the device edges and the number of photons absorbed from the large area surface. For this purpose, we coupled the perimeter edges of the LSCs to calibrated-Si-solar cells (IXYS KXOB22-12 × 1F, Open circuit voltage = 0.63 V, Fill factor = 0.7, External quantum efficiency ≈ 94%) and illuminated the LSCs with a solar simulator (100 mW cm⁻²) perpendicular to their top surface (108 cm² for both devices) in the absence of a reflector or back diffuser positioned at the bottom of the waveguide. The complete experimental setup is sketched in Figure 4, while the detailed description of the LSC performance characterization is reported in Methods section. Thereby, we measured OPE values of 3.8 ± 0.2% and 3.5 ± 0.2% and OQE values of 24.1 ± 0.4% and 27.4 ± 0.4%, for the LSCs based on GSH-OLA/OA and MPA-OLA/OA AIS/ZnS QDs, respectively, as shown in Table 1.^[29] These values are in the same order of magnitude as reported by Chen et al. employing, however, AIS QDs synthesized in an

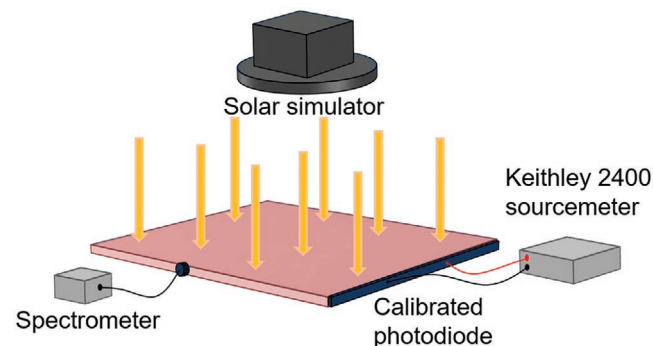


Figure 4. Experimental set-up for the efficiency measurement of AIS/ZnS-based LSC.

Table 1. Optical efficiency of $10.4 \times 10.4 \times 0.2 \text{ cm}^3$ LSC devices based on GSHOLA/OA and MPA-OLA/OA AIS/ZnS QDs.

Property	GSH-OLA/OA LSC	MPA-OLA/OA LSC
Optical power efficiency (OPE)		
$OPE = \frac{\# \text{ edge-emitted photons}}{\# \text{ total incident photons}}$	$3.8 \pm 0.2\%$	$3.5 \pm 0.2\%$
quantum optical efficiency (QOE)		
$QOE = \frac{\# \text{ edge-emitted photons}}{\# \text{ total absorbed photons}}$	$24.1 \pm 0.4\%$	$27.4 \pm 0.4\%$
$P_{\text{int}} = \frac{\text{edge emitted power}}{\text{absorbed power}}$	$16.9 \pm 0.4\%$	$17.9 \pm 0.4\%$

organic solvent with hazardous chemicals.^[17a] In addition, the electrical efficiency of the device coupled to a PV cell was used to evaluate the performance of the LSC devices. This property depends also on the conversion capacity of the PV cell.

The output power extracted from one of the LSC edges, and the respective fraction of the solar spectra absorbed by the utilized QDs are highlighted in Figures S7 and S8, Supporting Information. The obtained optical efficiencies are very promising considering that the devices preserve transparencies of 69% and 74% in the visible range of the solar spectrum (400–700 nm) and that the optical properties of the QDs are not yet optimized (PL QY = 70%). These results are in line with the performance of other devices^[11,12,16,17,21] of comparable dimensions,^[16,21,30,31,32,29] and with a similar degree of transparency (an overview of some of these devices is shown in Table S5, Supporting Information). As shown in Table 1, the LSC prepared with GSH based AIS/ZnS QDs performs slightly better than the LSC derived from initially MPA-capped AIS/ZnS QDs despite the red shifted emission band of the MPA-based QDs (see Figure 2). However, the overall losses of the MPA synthesis based AIS/ZnS QDs are lower than for the GSH synthesis based one (see Figure 3).

3. Conclusion

In a first proof-of-concept study, we realized large area, low cost, and highly efficient luminescent solar concentrators based on heavy-metal free AIS/ZnS QDs embedded in poly(lauryl) methacrylate utilizing simple preparation procedures. The QDs were synthesized in water using a simple two steps heating up synthesis or a microwave assisted synthesis approach. Independent of the stabilizing ligand used, that is, 3-mercaptopropionic acid and glutathione, the hydrophilic QDs show optical properties well suited for the application in LSCs like well separated absorption and emission bands and high photoluminescence quantum yield values of up to 65% in water and 74% in toluene after ligand exchange with hydrophobic oleylamine and oleic acid. First screening studies of the long-term stability of the toluene dispersions of the hydrophobic QDs utilized for LSC preparation suggest that the hydrophobic AIS/ZnS QDs remain stable in toluene for ≈ 2 years when stored at room temperature in the dark. Embedding both types of AIS/ZnS QDs in

PLMA with a simple photopolymerization approach provided transparent and highly emissive waveguides with photoluminescence quantum yields of at least 60% and a transparency of about 80% in the visible wavelength region. Utilization of these AIS/ZnS QDs in LSC devices yielded high optical power efficiencies of 3.8% and 3.5% equalling power quantum efficiencies of 24.1% and 27.4%, respectively, when considering the number of absorbed photons. These values can be further increased by optimizing the synthesis and fine-tuning the absorption and emission features, thereby further increasing the photoluminescence quantum yield, minimizing reabsorption and increasing the compatibility with the coupled solar cell as done by Anand et al.^[33]

The low cost of the materials, the simple and green synthesis, that can be easily upscaled, the excellent optical properties of the AIS/ZnS QDs, and the high efficiency of the devices underline the generally high potential of AIS/ZnS QDs for LSC technology. Furthermore, the parameters previously mentioned, and the low oxygen sensitivity of the process make these QDs candidates for a sustainable synthetic process. Parameters to further improve the performance of these promising materials include the modification of the ratio of the different constituents used for QD synthesis, QD size, and QD surface chemistry. Also, the doping of these AIS/ZnS QDs with other elements like Mn could be assessed as done for Pb-based QDs.^[30]

Supporting Information

Supporting Information is available from the Wiley Online Library or from the author.

Acknowledgements

L.D. and U.R.G. gratefully acknowledge financial support by the German Research Council (DFG; grant RE 1203/12-3). K.D.W. acknowledges the European Union's Horizon 2020 research and innovation program under the Marie Skłodowska-Curie grant agreement No. 846764. F.C. and S.B. thank the MIUR "Dipartimento di Eccellenza 2017 Project—Materials for Energy". The authors are very grateful to Dr. Oleksandr Stroyuk and Dr. Alexandra Raevskaya for their advice with the synthesis of AIS/ZnS QDs, to Dipl.-Ing. Arne Güttler for help with the instrumentation, to José Soares for fruitful discussions, and to Robert Voigt for software implementation. The authors acknowledge Dr. Ines Häusler for the TEM measurements, Mrs. Sigrid Benemann for the EDX analysis, and the MIB-SOLAR Laboratory for the use of their solar simulator. The TEM images were carried out as part of the DFG core facility project "Berlin Electron Microscopy Network (Berlin EM Network)".

Open access funding enabled and organized by Projekt DEAL.

Conflict of Interest

The authors declare no conflict of interest.

Data Availability Statement

Research data are not shared.

Keywords

luminescent solar concentrators, quantum dots, photovoltaics, AlS/ZnS, photoluminescence, microwave-assisted synthesis, thiol ligands

Received: March 22, 2021

Revised: May 11, 2021

Published online:

- [1] a) S. Sadeghi, R. Melikov, H. B. Jalali, O. Karatum, S. B. Srivastava, D. Conkar, E. N. Firat-Karalar, S. Nizamoglu, *ACS Appl. Mater. Interfaces* **2019**, *11*, 8710; b) M. G. Debije, P. P. C. Verbunt, *Adv. Energy Mater.* **2012**, *2*, 12.
- [2] a) T. B. Reed, R. M. Lerner, *Science* **1973**, *182*, 1299; b) W. H. Weber, J. Lambe, *Appl. Opt.* **1976**, *15*, 2299.
- [3] W. G. J. H. M. van Sark, K. W. J. Barnham, L. H. Slooff, A. J. Chatten, A. Buchtemann, A. Meyer, S. J. McCormack, R. Koole, D. J. Farrell, R. Bose, E. E. Bende, A. R. Burgers, T. Budel, J. Quilitz, M. Kennedy, T. Meyer, C. D. M. Donega, A. Meijerink, D. Vanmaekelbergh, *Opt. Express* **2008**, *16*, 21773.
- [4] F. Meinardi, F. Bruni, S. Brovelli, *Nat. Rev. Mater.* **2017**, *2*, 17072.
- [5] M. Saifullah, J. Gwak, J. H. Yun, *J. Mater. Chem. A* **2016**, *4*, 8512.
- [6] H. G. Zhao, Y. F. Zhou, D. Benetti, D. L. Ma, F. Rosei, *Nano Energy* **2017**, *37*, 214.
- [7] K. F. Wu, H. B. Li, V. I. Klimov, *Nat. Photonics* **2018**, *12*, 105.
- [8] P. Moraitis, R. E. I. Schropp, W. G. J. H. M. van Sark, *Opt. Mater.* **2018**, *84*, 636.
- [9] a) K. Nikolaidou, S. Sarang, C. Hoffman, B. Mendewala, H. Ishihara, J. Q. Lu, B. Ilan, V. Tung, S. Ghosh, *Adv. Opt. Mater.* **2016**, *4*, 2126; b) M. Y. Wei, F. P. G. de Arguer, G. Walters, Z. Y. Yang, L. N. Quan, Y. Kim, R. Sabatini, R. Quintero-Bermudez, L. Gao, J. Z. Fan, F. J. Fan, A. Gold-Parker, M. F. Toney, E. H. Sargent, *Nat. Energy* **2019**, *4*, 197; c) H. G. Zhao, D. Benetti, X. Tong, H. Zhang, Y. F. Zhou, G. J. Liu, D. L. Ma, S. H. Sun, Z. M. M. Wang, Y. Q. Wang, F. Rosei, *Nano Energy* **2018**, *50*, 756; d) H. G. Zhao, R. J. Sun, Z. F. Wang, K. F. Fu, X. Hu, Y. H. Zhang, *Adv. Funct. Mater.* **2019**, *29*, 1902262.
- [10] U. Resch-Genger, M. Grabolle, S. Cavaliere-Jaricot, R. Nitschke, T. Nann, *Nat. Methods* **2008**, *5*, 763.
- [11] K. Barnham, J. L. Marques, J. Hassard, P. O'Brien, *Appl. Phys. Lett.* **2000**, *76*, 1197.
- [12] a) J. M. Pietryga, R. D. Schaller, D. Werder, M. H. Stewart, V. I. Klimov, J. A. Hollingsworth, *J. Am. Chem. Soc.* **2004**, *126*, 11752; b) G. V. Shcherbatyuk, R. H. Inman, C. Wang, R. Winston, S. Ghosh, *Appl. Phys. Lett.* **2010**, *96*, 191901; c) L. Tan, Y. F. Zhou, F. Q. Ren, D. Benetti, F. Yang, H. G. Zhao, F. Rosei, M. Chaker, D. L. Ma, *J. Mater. Chem. A* **2017**, *5*, 10250.
- [13] European Union, EU RoHS 2 (Directive 2011/65/EU), *Official J. Eur. Union* **2011**, *54*, 1; https://doi.org/10.3000/17252555.L_2011.174.eng.
- [14] Y. X. Li, P. Miao, W. Zhou, X. Gong, X. J. Zhao, *J. Mater. Chem. A* **2017**, *5*, 21452.
- [15] S. Sadeghi, H. B. Jalali, R. Melikov, B. G. Kumar, M. M. Aria, C. W. Ow-Yang, S. Nizamoglu, *ACS Appl. Mater. Interfaces* **2018**, *10*, 12975.
- [16] F. Meinardi, S. Ehrenberg, L. Dharmo, F. Carulli, M. Mauri, F. Bruni, R. Simonutti, U. Kortshagen, S. Brovelli, *Nat. Photonics* **2017**, *11*, 177.
- [17] a) W. Chen, J. Li, P. Liu, H. Liu, J. Xia, S. Li, D. Wang, D. Wu, W. Lu, X. W. Sun, K. Wang, *Sol. RRL* **2017**, *1*, 1700041; b) I. V. Martynenko, A. S. Baimuratov, F. Weigert, J. X. Soares, L. Dharmo, P. Nickl, I. Doerfel, J. Pauli, I. D. Rukhlenko, A. V. Baranov, U. Resch-Genger, *Nano Res.* **2019**, *12*, 1595.
- [18] Y. M. You, X. Tong, W. H. Wang, J. C. Sun, P. Yu, H. N. Ji, X. B. Niu, Z. M. M. Wang, *Adv. Sci.* **2019**, *6*, 1801967.
- [19] Z. Li, X. Zhao, C. Huang, X. Gong, *J. Mater. Chem. C* **2019**, *7*, 12373.
- [20] C. Li, W. Chen, D. Wu, D. H. Quan, Z. M. Zhou, J. J. Hao, J. Qin, Y. W. Li, Z. B. He, K. Wang, *Sci. Rep.* **2015**, *5*, 17777.
- [21] F. Meinardi, H. McDaniel, F. Carulli, A. Colombo, K. A. Velizhanin, N. S. Makarov, R. Simonutti, V. I. Klimov, S. Brovelli, *Nat. Nanotech.* **2015**, *10*, 878.
- [22] M. B. Zhu, Y. X. Li, S. Q. Tian, Y. Xie, X. J. Zhao, X. Gong, *J. Colloid Interface Sci.* **2019**, *534*, 509.
- [23] O. Stroyuk, A. Raevskaya, F. Spranger, O. Selyshchev, V. Dzhagan, S. Schulze, D. R. T. Zahn, A. Eychmüller, *J. Phys. Chem. C* **2018**, *122*, 13648.
- [24] O. Stroyuk, F. Weigert, A. Raevskaya, F. Spranger, C. Wurth, U. Resch-Genger, N. Gaponik, D. R. T. Zahn, *J. Phys. Chem. C* **2019**, *123*, 2632.
- [25] a) C. Wurth, M. Grabolle, J. Pauli, M. Spieles, U. Resch-Genger, *Anal. Chem.* **2011**, *83*, 3431; b) C. Wurth, C. Lochmann, M. Spieles, J. Pauli, K. Hoffmann, T. Schuttrigkeit, T. Franzl, U. Resch-Genger, *Appl. Spectrosc.* **2010**, *64*, 733; c) C. Wurth, J. Pauli, C. Lochmann, M. Spieles, U. Resch-Genger, *Anal. Chem.* **2012**, *84*, 1345.
- [26] O. Chen, J. Zhao, V. P. Chauhan, J. Cui, C. Wong, D. K. Harris, H. Wei, H.-S. Han, D. Fukumura, R. K. Jain, M. G. Bawendi, *Nat. Mater.* **2013**, *12*, 445.
- [27] *Core/Shell Quantum Dots: Synthesis, Properties and Devices* (Eds: X. Tong, Z. M. Wang), Lecture Notes in Nanoscale Science and Technology, Vol. 28, Springer Nature Switzerland AG, Cham **2020**.
- [28] K. Connelly, Y. P. Wu, J. Chen, Y. Lei, *Appl. Energy* **2016**, *182*, 331.
- [29] M. G. Debije, R. C. Evans, G. Griffini, *Energy Environ. Sci.* **2021**, *14*, 293.
- [30] W. Liu, Q. Lin, H. Li, K. Wu, I. Robel, J. M. Pietryga, V. I. Klimov, *J. Am. Chem. Soc.* **2016**, *138*, 14954.
- [31] a) T. Cai, J. Wang, W. Li, K. Hills-Kimball, H. Yang, Y. Nagaoka, Y. Yuan, R. Zia, O. Chen, *Adv. Sci.* **2020**, *7*, 2001317; b) S. J. Gallagher, B. Norton, P. C. Eames, *Sol. Energy* **2007**, *81*, 813.
- [32] J. Roncali, *Adv. Energy Mater.* **2020**, *10*, 2001907.
- [33] A. Anand, M. L. Zaffalon, G. Gariano, A. Camellini, M. Gandini, R. Brescia, C. Capitani, F. Bruni, V. Pinchetti, M. Zavelani-Rossi, F. Meinardi, S. A. Crooker, S. Brovelli, *Adv. Funct. Mater.* **2019**, *30*, 1906629.